Int. J. Therm. Sci. (1999) 38, 481–491

An electromagnetic–thermal coupling example solved on a high frequency inductive system with the Matlab finite elements solver

Roland Ernst*, Philippe Grosse, Laurent Philippe

Laboratoire EPM-Madylam, 1340, rue de la Piscine, Domaine Universitaire, 38402-Saint-Martin-d'Hères, France
Département Optronique, Leti-CEA, 17, rue des Martyrs, 38054 Grenoble cedex 9, France

(Received 15 May 1998, accepted 26 October 1998)

Abstract — The simple SiC crystals inductive elaboration process is useful for specific devices working in electronic and optoelectronic areas. The SiC powder material is placed at the bottom of a graphite crucible and is inductively heated for out-gassing at about 1 600 °C in a controlled atmosphere. The SiC vapour is then transported to a condensation area on the top of the crucible where it condenses on a seed, forming a single crystal. The optimisation of this type of process requires numerical modelling. In this paper, a new and original electromagnetic-thermal coupling modelling tool based on the Matlab two-dimensional finite elements solver is presented. The electromagnetic model based on an 'inductor voltage imposed' equation gives the real inductor current density distribution, the impedance and coupling efficiency of the inductive system and the volume power density distribution in the induced charges such as the graphite crucible and holder and the surrounding insulating foam. The coupling with the thermal model is then achieved by taking this power density as the heat source on the right hand side in the energy equation. The temperature distribution issues from this coupling. The electrical and thermal results are in good agreement with measured values. This work shows that the Matlab mathematical and graphical efficiency associated with its finite elements solver builds an interesting tool for electrical and thermal design and optimisation of middle or high frequency inductive industrial processes. © Elsevier, Paris.

induction system / crystal growth / elaboration process / finite elements solver / electromagnetic-thermal coupling

Résumé — Un exemple de couplage électromagnétique-thermique résolu sur un système à induction haute fréquence à l'aide du solveur d'éléments finis de Matlab est présenté. Le procédé d'élaboration par induction de monocristaux de SiC est utilisé pour certains équipements spécifiques dans le domaine de l'électronique et de l'optoélectronique. La poudre de SiC est disposée au fond d'un creuset en graphite et est chauffée par induction à une température de l'ordre de 1 600 °C en atmosphère contrôlée pour la phase de dégazage. Les vapeurs de SiC sont ensuite transportées vers une zone de condensation en partie supérieure du creuset où elles se condensent sur un germe, en formant un monocristal. L'optimisation de ce type de procédé requiert une phase de modélisation numérique. Dans cet article, un nouvel outil original de modélisation numérique du couplage électromagnétique-thermique basé sur l'utilisation du solveur d'éléments finis bidimensionnel de Matlab est présenté. Le modèle électromagnétique basé sur une équation en «tension d'inducteur imposée» donne la distribution réelle de la densité de courant, l'impédance et le rendement de couplage du système à induction, ainsi que la distribution de la puissance volumique dans les charges induites, comme le creuset en graphite, le support en graphite et le feutre de graphite isolant entourant l'ensemble. Le couplage avec le modèle thermique est ensuite obtenu en considérant la puissance volumique comme la source de chaleur dans le second membre de l'équation de l'énergie. La distribution de température est issue de ce couplage. Les résultats des modélisations électromagnétique et thermique sont en bon accord avec les mesures. Ce travail montre que l'efficacité mathématique et graphique de Matlab, associée avec son solveur d'éléments finis, constitue un outil intéressant d'aide à la conception et à l'optimisation de procédés inductifs industriels moyenne et haute fréquence. © Elsevier, Paris.

système à induction / croissance cristalline / procédés d'élaboration / solveur d'éléments finis / couplage électromagnétique-thermique

Nomenclature

a	coefficient of the Matlab generic equation	
A	vector potential	$Wb \cdot m^{-1}$
B	magnetic induction	T
c	coefficient of the Matlab generic equation	
C	capacity connected to the inductor	F

* Roland.Ernst@polycnrs-gre.fr

D_5,D_6,D_7,D_8,D_{10}	difference between mean current I_{mean} and each turn current	A
E	electric field	$V \cdot m^{-1}$
f	coefficient of the Matlab generic equation	
h	convection coefficient	$W \cdot m^{-2} \cdot K^{-1}$
i	complex square root of -1	
I_5,I_6,I_7,I_8,I_{10}	current in each inductor turn	A
j	current density	$A \cdot m^{-2}$
k	thermal conductivity	$W \cdot m^{-1} \cdot K^{-1}$
L	inductance	H
n	unity vector normal to the boundary	
r	radial co-ordinate of the cylindrical co-ordinates system	m
R	electrical resistance	Ω
relax	relaxation coefficient for currents equilibration calculation	
t	time	s
T	temperature	K
u	unknown of the Matlab generic equation	
U	current turn voltage	V
$U_5, U_6, U_7, U_8, U_{10}$	voltage of each inductor turn	V
V	electric scalar potential	
x	x-co-ordinate of the Cartesian co-ordinates system	m
x_i	x-co-ordinate of the power density calculation grid nodes	m
y	y-co-ordinate of the Cartesian co-ordinates system	m
y_i	y-co-ordinate of the power density calculation grid nodes	m
z	axial co-ordinate of the cylindrical and Cartesian co-ordinates system	m
$Z_5, Z_6, Z_7, Z_8, Z_{10}$	impedance of each inductor turn	Ω

Subscripts

A_θ	orthoradial component of vector potential	$Wb \cdot m^{-1}$
A^*_θ	complex conjugate of A_θ	$Wb \cdot m^{-1}$
E_θ	orthoradial component of electric field vector	$V \cdot m^{-1}$
f_r	working frequency	Hz
I_a	anode current	A
I_i	inductor current for measurements	A
I_{mean}	mean value of the inductor turn currents	A
j_θ	orthoradial component of current density	$A \cdot m^{-2}$
k_f	thermal graphite foam conductivity	$W \cdot m^{-1} \cdot K^{-1}$
k_g	thermal graphite conductivity	$W \cdot m^{-1} \cdot K^{-1}$
T_{amb}	ambient temperature	K
T_{ref}	reference temperature for radiative losses	
U_t	total inductor voltage	V
V_a	anode voltage	V
V_{oc}	inductor voltage	V
T_A,T_B,T_C,T_D	temperature at points A, B, C, D	K

Greek symbols

ε	emissivity	
μ	magnetic permeability	$H \cdot m^{-1}$
θ	angular co-ordinate of the cylindrical co-ordinates system	rd
ρ	electrical resistivity	$\Omega \cdot m$
ρ_f	graphite foam electrical resistivity	$\Omega \cdot m$
ρ_g	graphite electrical resistivity	$\Omega \cdot m$
σ	electrical conductivity	$\Omega^{-1} \cdot m^{-1}$
σ_{st}	Stefan-Boltzmann constant	$W \cdot m^{-2} \cdot K^{-4}$
ω	angular frequency	$rd \cdot s^{-1}$
ψ	volumic power density	$W \cdot m^{-3}$

1. INTRODUCTION

The elaboration of single crystals of SiC is useful for some specific devices in electronic and optoelectronic areas. The proper working of these devices requires good crystal quality. Many efforts have been made in recent years to improve this quality by developing special elaboration processes [1–4].

The elaboration process concerned in this paper is based on the heating by induction of the SiC powder material in a sealed furnace at a temperature higher than 1 800 K and a pressure lower than $5 \cdot 10^3$ Pa. The SiC which is placed at the bottom of a graphite container is then sublimated in an inert gas and transported onto the upper colder face where its condensation is initiated on a seed placed in a precise spot. Thus it is possible to obtain a single crystal. The above-mentioned temperature of 1 800 K is related to the out-gassing phase which is considered in this paper.

The different experiments which have been done show that the quality of the crystal depends on many parameters which must be taken into account in such a process. From a 'microscopic' point of view, when for instance analysing the crystal growth, phenomena such as physical vapour transport and chemical reactions must be studied. But from a 'macroscopic' point of view, for instance for the global design of the furnace, these phenomena can be simplified and only electromagnetic and thermal aspects have to be studied, which is the case in this paper.

The work presented in this paper corresponds to this 'macroscopic' point of view: its purpose is the use of the Matlab finite elements solver for solving the coupling of electromagnetism and heat transfer in the furnace. This electromagnetic-thermal modelling is specifically useful for the electrical part of the design of this furnace and also gives interesting data about the temperature gradient in the furnace which is required in order to obtain a correct sublimation and condensation of the SiC. Thus it gives the guidelines for a proper global design of such a process.

Many publications have been written concerning the finite elements method, about both the theory [5, 6] and its applications for electromagnetic modelling [7] and electromagnetic-thermal coupling [8]. Thus the finite elements method will not be presented again here. But with the presentation of the electromagnetic-thermal steady state model, the main original advantages of using the Matlab environment and its included finite elements solver (Partial Differential Equations Toolbox) will be shown. It must be clearly noted that the aim of this work is not to optimise the finite elements methods but to use the Matlab finite elements solver as a help for studying the SiC crystal growth process from a electromagnetic and thermal point of view. The main steps of this modelling process with the corresponding original points may be described as follows: first, the electromagnetic equation whose unknown is the orthoradial component of the vector potential at each point, is solved including a right hand side source term which is related to the inductor voltage imposed by the generator. This allows the real inductor current density distribution to be determined in each turn and also the distribution of the induced current density in the different induced materials. This solving mode shows clearly the proximity effects between the turns themselves and between the turns and the charges implying a non regular distribution of the inductor current density in each turn. By integration of this current density in each turn, the inductor current is obtained, giving the complex impedance of the system, i.e. its resistance and its reactance which are useful for the electrical aspects. Then the induced power density issuing from the current density is determined at each mesh point of the induced pieces. This power density is then extrapolated for each node of the thermal mesh and becomes the source term of the thermal equation which is also solved by finite elements. Finally the temperature repartition in the concerned materials is obtained. The boundary conditions involving convection and radiation losses or imposed temperature are fixed by generalised Neuman or Dirichlet conditions. In the electromagnetic equation the resistivity of the materials is constant and equal to its value corresponding to the estimated mean temperature. In the thermal equation, the thermal conductivity is dependent on the temperature. The electrical and thermal results issuing from this model are compared with experimental measures made on the real process which is in a development stage. The different steps of this electromagnetic-thermal modelling preceded by a presentation of the process and the corresponding experimental measurements are presented in the following parts of this paper.

2. PRESENTATION OF THE PROCESS

The main part of the process is sketched in *figure 1*. The silicon carbide (SiC) powder which must be heated and sublimated is placed at the bottom of a graphite crucible whose top includes a SiC seed on a condensation area on which a single crystal grows by condensation of the transported vapour. This crucible is surrounded by a thermal insulating graphite foam which is fitted with holes at the top and the bottom, thus allowing pyrometric measurements. An additional graphite holder is set under the foam.

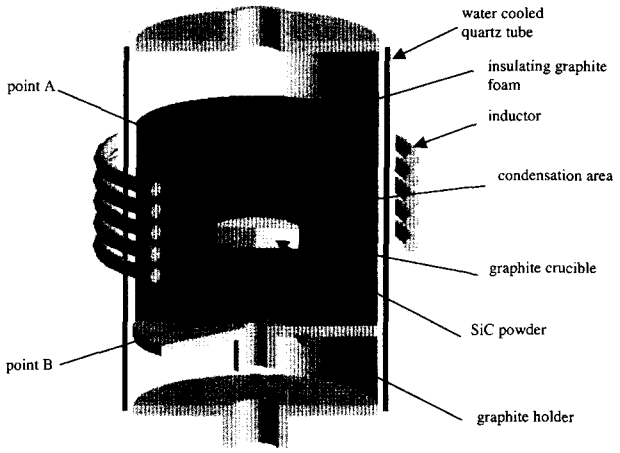

Figure 1. Diagram of the process.

A water-cooled double jacket quartz tube is set around the crucible and the insulating foam so that, thanks to two top and bottom flanges, the heating and sublimation processes are achieved in an argon controlled atmosphere.

A heating inductor is placed around the quartz tube. This water-cooled five turn copper inductor is connected to a capacity battery forming a parallel oscillating circuit which is connected to a 50 kW high frequency triode generator with a 114 kHz working frequency.

In order to obtain a single crystal growth by condensation of the SiC vapours on the seed placed on the top of the graphite crucible, the estimated temperature in the corresponding area is about 1 600 to 1 800 °C. This shows one of the major points of the numerical model: after validation of this model by the only two external measured temperatures at points A and B of *figure 1*, it is then possible to know, thanks to this theoretical modelling, the temperature inside the graphite crucible where any experimental measurement is difficult to obtain.

3. MEASUREMENTS RESULTS ON THE INSTALLATION

In order to validate the electromagnetic-thermal modelling of the furnace, some electrical and thermal measurements were made on the device.

The simplified electrical sketch of the inductor connection to the triode generator is given in *figure 2*. The working frequency is 114 kHz. The inductor is connected in parallel with a set of five 3 μF capacitors connected in series and forming a capacitive potential divider, the generator being connected at the ends of three of these capacitors. This assumes a correct impedance adaptation. The whole capacity value of the five series capacitors connected to the inductor including the furnace is $C = 0.6$ μF. These capacitors form a self-oscillating circuit with the inductor.

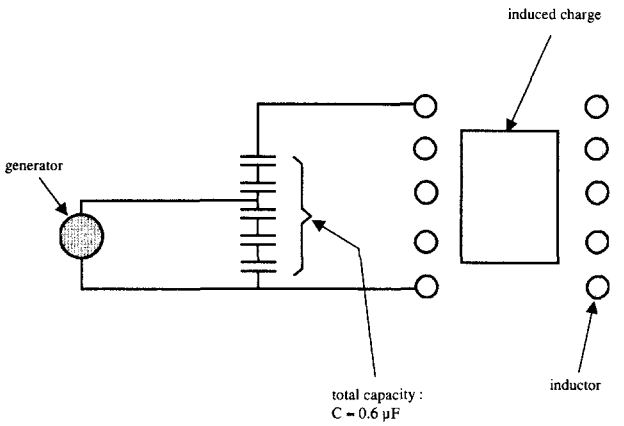

Figure 2. Induction system connection to the generator.

First, after disconnecting the generator, the capacity C is connected to an impedance measurement device based on a self-resonant capacity discharge method [9]. These impedance measurements without the furnace inside the inductor (inductor alone) and with the furnace inside the inductor (inductor + furnace) are outlined in *table I*.

TABLE I
Measured inductance, resistance, and quality factor in the installation.

	Frequency	Inductance	Resistance	Quality factor
Inductor alone	103 kHz	3.95 μH	30 mΩ	88
Inductor + furnace	114 kHz	3.2 μH	109 mΩ	21

The resistance measured without and with the furnace gives the coupling efficiency of the furnace which is about 64 %.

Then the triode generator is connected to the oscillating circuit formed by the capacitors and the inductor with the furnace inside it, and, for the anode voltage V_a set to 2 kV, the corresponding anode current I_a, inductor voltage V_{oc} and inductor current I_i are measured, and are given in *table II*.

Finally, for several values of the anode voltage, the temperatures T_A and T_B at the top and the bottom of the crucible (points A and B in *figure 1*) are measured by pyrometer through the holes in the graphite foam. The measured values are given in *table III*.

TABLE II
Measured anode DC voltage and current and inductor AC voltage and current in the installation.

Anode voltage V_a	Anode current I_a	Inductor voltage V_{oc}	Inductor current I_i
2 kV	2 A	353 V_{rms}	152 A_{rms}

TABLE III
Measured temperature of upper and lower points A and B for different anode voltages and currents.

Anode voltage V_a (kV)	Anode current I_a (A)	Upper temperature T_A (°C)	Lower temperature T_B (°C)
2	2	1 700	1 668
2.4	2.5	2 000	1 910
3	3.2	2 250	2 103

These measured electrical and thermal values are used for the validation of the electromagnetic-thermal model. The accuracy of these measurements is estimated to about 5 %.

4. THE ELECTROMAGNETIC MODEL

4.1. Properties of the materials

The resistivities of the graphite crucible and holder, and of the graphite foam are assumed to be constant and equal to the value corresponding to the estimated mean temperature of the materials, meaning 1 500 °C for the crucible and 1 000 °C for the foam. According to the literature [10], the values of $\rho_g = 1.538 \cdot 10^{-5} \Omega \cdot m$ for the graphite crucible and holder resistivity and of $\rho_g = 2.3 \cdot 10^{-3} \Omega \cdot m$ for the graphite foam resistivity are used.

4.2. The electromagnetic equation

As the problem is axisymmetric, a cylindrical coordinates system (r, θ, z) is used. The electromagnetic equation is derived from the Maxwell equations with the

following unknowns, which are the complex amplitudes (of the corresponding sinusoidal time-dependant fields):

- $\vec{B}$: magnetic induction vector
- $\vec{j}$: current density
- $\vec{E}$: electric field
- $\vec{A}$: magnetic vector potential
- V: electric scalar potential.

All these unknowns (except for V) do not depend on the θ co-ordinate ($\partial/\partial\theta = 0$). $\vec{B}$ has two components along r and z, and $\vec{j}$, $\vec{E}$ and $\vec{A}$ have only an orthoradial component, respectively called j_θ, E_θ and A_θ. The scalar potential V only varies linearly with θ for the inductor turns with a corresponding constant orthoradial component of the potential gradient $\overrightarrow{\text{grad}}V$ equal to $U/(2\pi r)$ where U is the turn voltage (issued from the generator) and r is the current radius. This gradient is zero in the other domains. The additional parameters involved in the Maxwell equations are the following:

- μ: magnetic permeability
- σ: electric conductivity
- ρ: electric resistivity (equal to $1/\sigma$)
- ω: electric pulsation ($\omega = 2\pi f_r$, where f_r is the frequency).

The Maxwell equations and Ohm's law giving the electromagnetic equation are the following:

$$\overrightarrow{\text{Rot}}\,\frac{\vec{B}}{\mu} = \vec{j} \tag{1}$$

$$\vec{B} = \overrightarrow{\text{Rot}}\,\vec{A} \tag{2}$$

$$\vec{j} = \sigma\,\vec{E} \tag{3}$$

$$\vec{E} = -\mathrm{i}\,\omega\,\vec{A} - \overrightarrow{\text{grad}}V \tag{4}$$

After combining the former equations and eliminating $\vec{B}$, $\vec{j}$ and $\vec{E}$ and after eliminating time, the orthoradial projection of the equation obtained including the unknown orthoradial component A_θ of the vector potential $\vec{A}$ may be written as follows :

$$-\frac{\partial}{\partial r}\left(\frac{1}{\mu}\,r\,\frac{\partial A_\theta}{\partial r}\right) - \frac{\partial}{\partial z}\left(\frac{1}{\mu}\,r\,\frac{\partial A_\theta}{\partial z}\right) + \left(\frac{1}{\mu\,r} + \mathrm{i}\,\frac{\omega}{\rho}\,r\right)A_\theta = -\frac{U}{2\pi\rho} \tag{5}$$

It must be noted that this equation is a punctual equation and that U is the voltage amplitude of each inductor turn. For all the other domains such as the induced materials, U, and thus also the right hand side of the equation, is zero.

The Matlab finite elements solver works only in a two-dimensional Cartesian co-ordinates system (xy). So in this Cartesian co-ordinates system and by assuming the correspondence between r and x and between z and y, the equation (5) may be written :

$$-\frac{\partial}{\partial x}\left(\frac{1}{\mu}\,x\,\frac{\partial A_\theta}{\partial x}\right) - \frac{\partial}{\partial y}\left(\frac{1}{\mu}\,x\,\frac{\partial A_\theta}{\partial y}\right) + \left(\frac{1}{\mu\,x} + \mathrm{i}\,\frac{\omega}{\rho}\,x\right)A_\theta = -\frac{U}{2\pi\rho} \tag{6}$$

Finally, by using the vector operators, this equation may be written:

$$-\text{div}\left(\frac{1}{\mu}\,x\,\overrightarrow{\text{grad}}\,A_\theta\right) + \left(\frac{1}{\mu\,x} + \mathrm{i}\,\frac{\omega}{\rho}\,x\right)A_\theta = -\frac{U}{2\pi\rho} \tag{7}$$

The equation (7) corresponds to the generic equation with the scalar unknown u suggested by the Matlab finite elements solver. This equation is:

$$-\text{div}(c\,\overrightarrow{\text{grad}}\,u) + a\,u = f \tag{8}$$

Thus the coefficients of this equation must be entered for each sub-domain as follows:

$$c = \frac{1}{\mu}\,x \tag{9}$$

$$a = \left(\frac{1}{\mu\,x} + \mathrm{i}\,\frac{\omega}{\rho}\,x\right) \tag{10}$$

$$f = -\frac{U}{2\pi\rho} \tag{11}$$

In the a coefficient the $1/x$ term could give a problem by becoming infinite when x tends to zero on the symmetry axis which is the case for the mesh triangles which have nodes on this axis. But as the Matlab solver uses a Gauss method the integrals are never calculated on the mesh nodes but inside these meshes, so that the integrals remain finite. Nevertheless it must be admitted that while this method gives an excellent accuracy for polynomial terms it is less accurate for a term like $1/x$.

It must be noted that, although it is not the case here, the coefficients c, a and f may be dependent on the unknown u (thus on A_θ) by using the non linear solver. It is for instance possible to take into account a non linear magnetic core whose permeability is given by a function of $\frac{1}{r}\left|\overrightarrow{\text{grad}}\,(r\,A_\theta)\right|$.

4.3. Geometry and boundary conditions

It may be assumed that the SiC powder itself, as it does not couple on the electromagnetic field, is not very influential in the study of the global electromagnetic and thermal aspects. So it has been removed from the studied system, which means that the graphite crucible inner chamber is considered as electromagnetically and thermally inactive (like a vacuum area).

The geometry entered in the Matlab finite elements solver is quite close to the real process geometry and is given in *figure 3*. Each sub-domain has a sub-domain number indicated in this figure. They are listed as follows :

- sub-domains 1 and 9: vacuum
- sub-domain 2: graphite crucible
- sub-domain 3: graphite holder
- sub-domain 4: graphite foam
- sub-domains 5, 6, 7, 8, 10: inductor copper turns.

The boundary condition is a Dirichlet condition expressed by imposing a zero value of the unknown A_θ at the external boundary corresponding to the ABCD rectangular contour in *figure 3*. This corresponds to an anti-symmetric condition on the AD revolution axis and to an A_θ vanishing to zero on the AB,BC and CD boundaries if they are far enough from the inductive system.

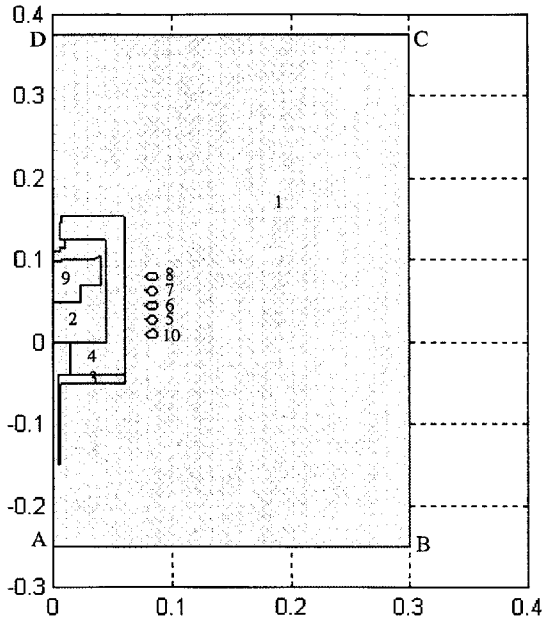

Figure 3. Electromagnetic model geometry.

4.4. First solving step and results

The whole domain is meshed by several successive refining operations into triangular meshes with the auto-adaptive mesh generator until there are about two triangles in the skin depth which is about 0.2 mm at the 114 kHz working frequency in the copper inductor turns (more than two triangles in the skin depth improves the results by only a few percent), thus giving a total amount of about 40 000 triangles.

The solving conditions correspond to the electrical experimental test detailed in *table II*. In this test the measured inductor voltage is 353 $V_{\rm rms}$ which is applied to the ends of the 5 series turns. So, for this first model solving step, the input voltage U per turn in the electromagnetic equation presented in part 4.2 is equal to the total measured voltage divided by 5, meaning 70.6 $V_{\rm rms}$. After solving, the orthoradial potential vector component A_θ is obtained for the whole of the studied domain. Consequently the above Ohm's law and Maxwell equations (3) and (4) give the current density in the 5 inductor turns corresponding to the 5 sub-domains 5, 6, 7, 8 and 10 in *figure 3*. This current density is integrated in each turn with the aid of a custom written integration function, implying the determination of the total current in each of the five inductor turns. These calculated currents, named I_5, I_6, I_7, I_8, I_{10} (the numbers correspond to the sub-domain numbers of *figure 3*) are schematically indicated in *figure 4*. These complex currents are mainly inductive with a major imaginary part, which is normal at this high working frequency, but they are not equal when they should be equal since the five turns are connected in series. Effectively the current module in the median turns is almost twice as small as the current module in the end turns with a normal vertical symmetry. This comes from the fact that on the one hand the inductance of each turn including the mutual inductance with the other turns is not the same, being smaller at the ends (turns 10 and 8) than in the middle (turn 6), and on the other hand this first solving step is performed with the same voltage U at the ends of each turn in the electromagnetic equation. That means that the solving method must be improved by taking into account the turn currents equality, thus implying the non equality of the U voltage on each turn in the electromagnetic equation. This is explained in the next section.

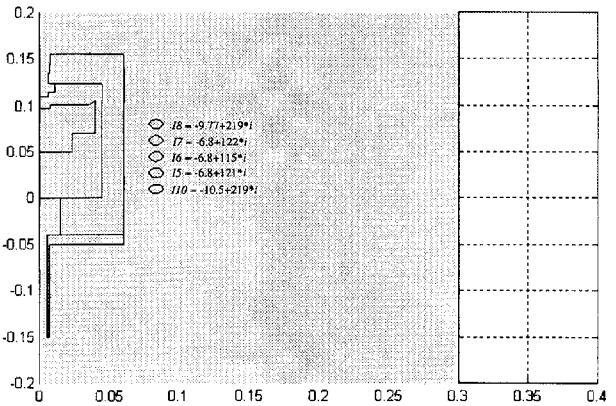

Figure 4. Turn currents calculated after first solution step.

4.5. Solving with currents equilibration

The turn currents equilibration will be obtained by a custom written 'equilibration' function which performs successive iterative solutions with a numerical voltage adjustment on each turn until current equilibration is obtained. The starting solution corresponds to the former first solving step with the same U voltage ($U = 70.6\ V_{rms}$) on each turn. The working flowchart of this equilibration function corresponds to a Jacobi method and is outlined in *figure 5* with the following naming of the electrical parameters related to the five turns which have sub-domain numbers 5, 6, 7, 8 and 10 (in *figure 4* above):

- U_5, U_6, U_7, U_8, U_{10}: voltages at the ends of each turn;
- I_5, I_6, I_7, I_8, I_{10}: turn currents;
- Z_5, Z_6, Z_7, Z_8, Z_{10}: impedance of each turn;

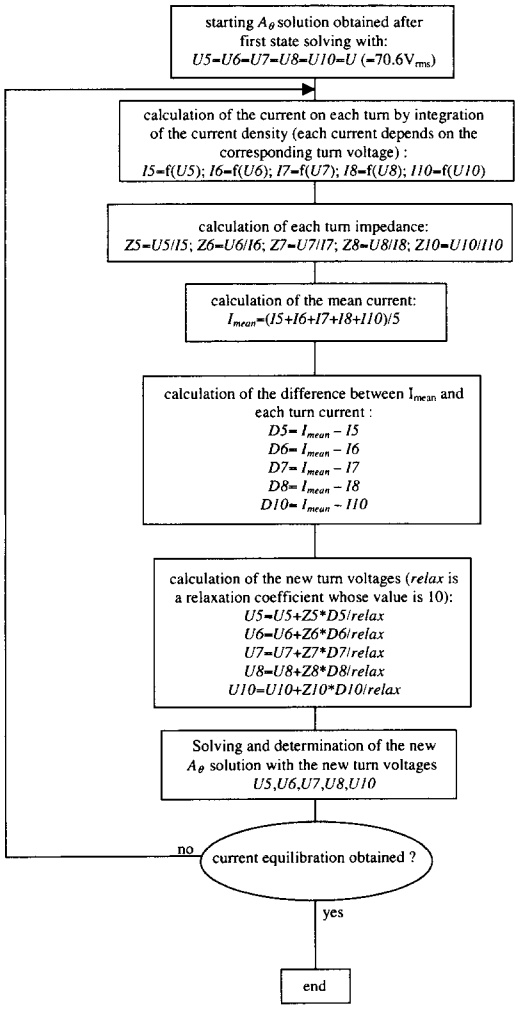

Figure 5. Flowchart of turn currents equilibration calculation.

- I_{mean}: mean value of the turn current;
- D_5, D_6, D_7, D_8, D_{10}: difference between I_{mean} and each turn current ($D_i = I_{mean} - I_i$ with $i = 5, 6, 7, 8, 10$).

Thus after less than 10 iterations, the equilibration of the turn currents is obtained with a set of turn voltages which are no longer equal, as represented in *figure 6*. Effectively these voltages (with a major real part) show a normal vertical symmetry and are greater in the middle ($U_6 = 77\ V_{rms}$) than at the ends ($U_8 = U_{10} = 64\ V_{rms}$). This calculated electrical working corresponds now to the real inductor working with the five turns connected in series.

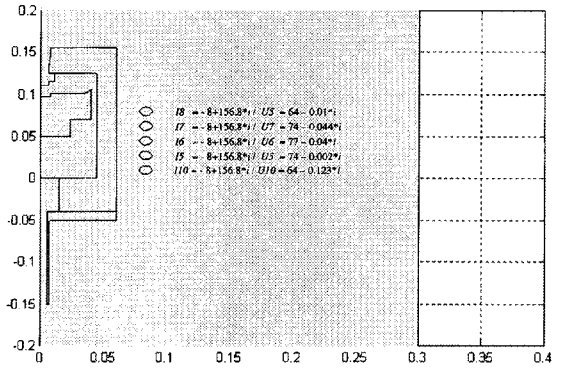

Figure 6. Turn currents and voltages obtained after current equilibration calculation.

4.6. Solving and results

After solving with current equilibration, some interesting results are obtained. First, *figure 7* gives a sketch of the field lines, obtained classically by drawing the lines of constant value of the A_θ module multiplied by the x co-ordinate.

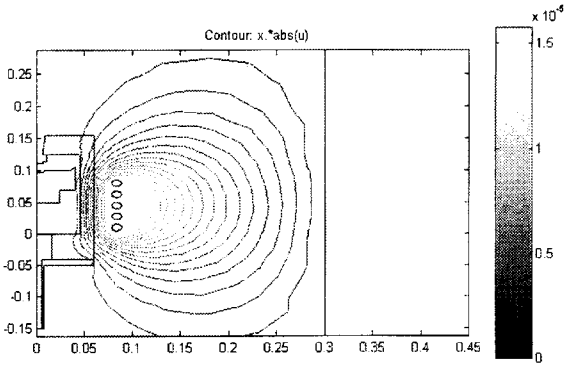

Figure 7. Magnetic field lines (obtained by drawing the A_θ module multiplied by the x co-ordinate - values going from 0 to $1.5 \cdot 10^{-5}$ Wb·m^{-1}).

The calculated inductor current module is 157 $A_{\rm rms}$, which is close to the measured current of 152 $A_{\rm rms}$ (*table II*). By adding the five calculated turn voltages U_5, U_6, U_7, U_8 and U_{10}, the total inductor voltage $U_{\rm t}$ is $353 - 0.052\ i\ (V_{\rm rms})$ which is very close to the measured 353 $V_{\rm rms}$ (*table II*). By dividing $U_{\rm t}$ by the inductor current, the following values of the global resistance R and inductance L are obtained :

- resistance: $R = 113\ \text{m}\Omega$
- inductance: $L = 3.14\ \mu\text{H}$

These values are also close to the measured values (*table I*, second line).

The current density distribution is also determined in each turn and this gives interesting information about this real distribution which is given in module form in *figure 8* on which the x axis is the radial direction and the y axis is the vertical axial direction. These axes are the same as those defined in section 4.2. It can be clearly seen that the current density exhibits a normal vertical symmetry (along Oy) and is contained all around each turn in the electromagnetic skin depth which is small at the 114 kHz working frequency (0.2 mm) compared with the turn diameter (10 mm). These results are typical. But the additional interesting point arising from this is the determination of the current density distribution around the turns cross section: it can be noted that the major part of the current density is located on the part of the turns perimeter which faces the revolution axis, with a shifting toward the top for the upper end turn 8 and toward the bottom for the lower end turn 10. All these factors mean that the inductor corresponding resistance is always much stronger at these middle or high AC working frequencies than during DC when the current density is evenly distributed in the cross section of each turn. This effect is called the 'proximity effect' and is due to inductive interactions between all of the turns and between the turns and the induced materials. Consequently it is important to note that the induced effects in the induced materials, such as the crucible, are strongly dependent on this real non uniform inductor current density distribution, which also has a considerable influence on later temperature determination.

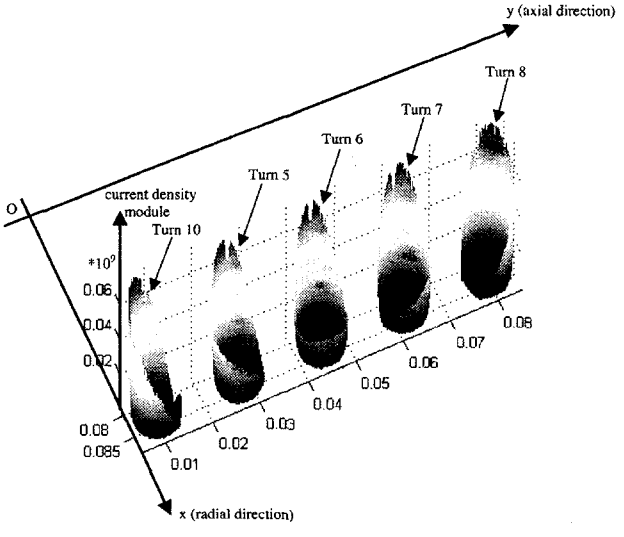

Figure 8. Current density module in the 5 inductor turns.

Finally, from the A_θ solution obtained which is now determined in each electrical conducting material of the studied domain, it is easy to determine the corresponding Joule induced volume power density Ψ by the following expression:

$$\psi = \sigma\, \omega^2\, A_\theta\, A_\theta^* \tag{12}$$

This power density is calculated with a custom written function on a rectangular grid which includes the induced materials, i.e. the graphite crucible and holder and the graphite foam, corresponding to the 2, 3 and 4 sub-domain numbers (on all the grid nodes which do not belong to the induced materials, Ψ is forced to zero). This power density will be used as the heat source term of the thermal equation and is represented in *figure 9* on which the x axis is the radial direction and the y axis is the vertical axial direction. It can be noted that the graphite crucible and holder and the graphite foam couple on the magnetic field with a major part in the crucible which must be the case in order to achieve an efficient heating of the SiC powder.

By integrating the volume power density Ψ on the whole volume of the graphite crucible and holder and the graphite foam the total induced power obtained is 2 275 W. This is in good agreement with the electrical measurements given in *table II* of § 3 corresponding to a $V_{\rm a} = 2$ kV anode DC voltage and a $I_{\rm a} = 2$ A anode DC current on the triode generator. The related DC net power is equal to $V_{\rm a}\, I_{\rm a}$, i.e. 4 000 W. After taking into account the classical 70 to 75 % generator efficiency and the 64 % inductor coupling efficiency issuing from the measurements given in *table I* (inductor alone and inductor + furnace) the remaining power directly

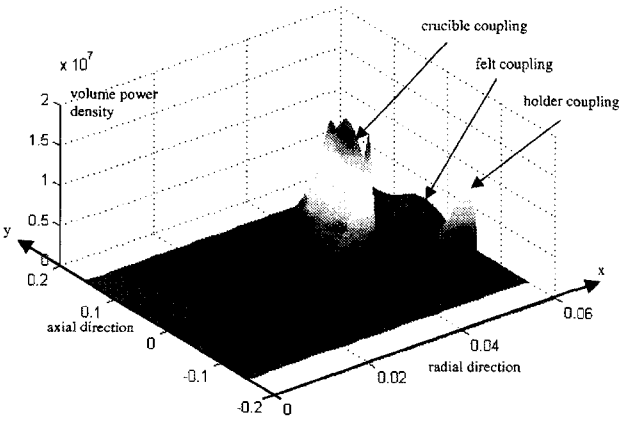

Figure 9. Volume power density repartition.

injected into the induced materials is about 2 000 W which is very close to the previously numerically calculated 2 275 W.

So it may be concluded at this step that the electromagnetic model gives results which are in good agreement with the experimental measurements and that it is possible to go further by setting up the thermal model which will be coupled to the electromagnetic model by use of the previously calculated Ψ volume power density as the heat source.

5. THE THERMAL MODEL

As stated above in § 4.6, the induced volume power density Ψ is calculated on a rectangular grid including the induced materials such as the graphite crucible, holder and foam. This calculation is made by a custom written function which extrapolates the A_θ solution obtained after solving on this rectangular grid and uses expression (12) to determine Ψ on each node (x_i, y_i) of this grid. The step of this grid is about 1 mm, which is obtained with 40 points for the x_i and 200 points for the y_i, giving a total amount of 8 000 points. This induced volume power density is the heat source for heating the furnace which is modelled by the thermal model which takes into account the graphite crucible, holder and foam. This thermal model is also set up by using the Matlab finite elements solver for solving the thermal equation as explained in the following steps.

5.1. Properties of the materials

The solid graphite crucible and holder have a good thermal conductivity implying a relatively small temperature gradient inside them. Thus their thermal conductivity k_g is constant and equal to the value of the graphite thermal conductivity at an estimated mean temperature of about 1 500 °C, i.e. 53 $W{\cdot}m^{-1}{\cdot}K^{-1}$. On the other hand, a strong temperature gradient is expected in the graphite insulating foam. The thermal conductivity k_f of this foam is therefore chosen as a function of the temperature T, which is the following expression, according to the bibliography [10]:

$$k_f = 0.17\,10^{-6}T^2 + 0.08 \quad (W{\cdot}m^{-1}{\cdot}K^{-1}) \qquad (13)$$

5.2. The thermal equation

As the problem is axi-symmetric, a cylindrical co-ordinates system (r, θ, z) is used as for the electromagnetic problem. The temperature T is the scalar unknown. The classical temperature diffusion equation where k is the thermal conductivity and ψ is the right hand side volume power density giving the heat source, is written as follows:

$$-\operatorname{div}(k\,\overrightarrow{\operatorname{grad}}\,T) = \psi \qquad (14)$$

By developing the divergence and gradient operators and by multiplying the two sides by the current radius r, this equation may be written as following:

$$-\frac{\partial}{\partial r}\left(k\,r\,\frac{\partial T}{\partial r}\right) - \frac{\partial}{\partial z}\left(k\,r\,\frac{\partial T}{\partial z}\right) = \psi\,r \qquad (15)$$

The Matlab finite elements solver works only in a two-dimensional Cartesian co-ordinates system (xy). Thus in this Cartesian co-ordinates system and by assuming the correspondence between r and x and between z and y, the equation (15) may be written :

$$-\frac{\partial}{\partial x}\left(k\,x\,\frac{\partial T}{\partial x}\right) - \frac{\partial}{\partial y}\left(k\,x\,\frac{\partial T}{\partial y}\right) = \psi\,x \qquad (16)$$

Finally, by using the vector operators, this local equation on each point (x,y) of the domain under consideration may be written:

$$-\operatorname{div}(k\,x\,\overrightarrow{\operatorname{grad}}\,T) = \psi\,x \qquad (17)$$

The equation (17) corresponds to the generic equation with the scalar unknown u suggested by the Matlab finite elements solver which is:

$$-\operatorname{div}(c\,\overrightarrow{\operatorname{grad}}\,u) + a\,u = f \qquad (18)$$

Thus the coefficients of this equation must be entered for each sub-domain as follows:

$$c = k\,x \qquad (19)$$

$$a = 0 \qquad (20)$$

$$f = \psi\,x \qquad (21)$$

As previously stated the thermal conductivity $k = k_f$ of the graphite foam is a function of the unknown temperature, which needs the use of the non linear solver. The right hand side of the equation $f = \psi x$ is directly a custom written function which interpolates the former volume power density Ψ obtained by solving the electromagnetic problem (§ 4.6) from the rectangular grid (x_i, y_i) to each current point (x, y) and which multiplies this power density by the current x co-ordinate.

5.3. The geometry and boundary conditions

The geometry entered in the Matlab finite elements solver is quite close to the real process geometry and is given in *figure 10.* Each sub-domain has a sub-domain

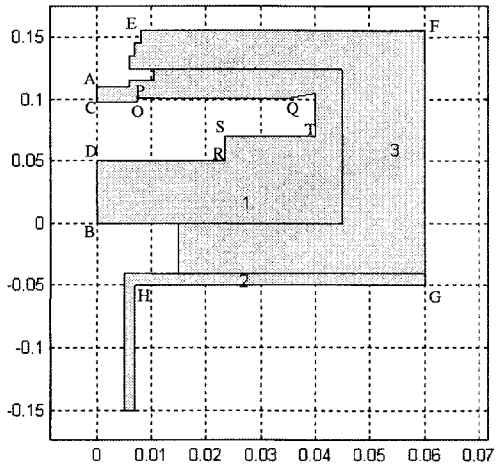

Figure 10. Thermal model geometry.

number indicated on this figure. They are listed as following:

- sub-domain 1: graphite crucible;
- sub-domain 2: graphite holder;
- sub-domain 3: graphite foam.

The set of boundary conditions is the following:

- on faces EF and GH: thermal flux generalised Neumann boundary conditions relative to convection losses expressed by $-k\,\vec{n}\,\overrightarrow{\text{grad}}\,T = h\,(T - T_{\text{amb}})$ with a convection coefficient $h = 5\ \text{W}\cdot\text{m}^{-2}\cdot\text{K}^{-1}$ and an estimated ambient temperature $T_{\text{amb}} = 773$ K (500 °C) ($\vec{n}$ is the normal vector on the boundary);
- on face FG: fixed temperature Dirichlet boundary conditions; this temperature is estimated at 773 K (500 °C);
- all the other faces are insulated (no losses) which is expressed by a zero thermal flux generalised Neumann boundary condition. As previously stated the SiC powder has been removed for simplification, which means that the surface of the graphite crucible internal chamber is considered as a boundary.

5.4. Solving and results

After meshing the three sub-domains with the auto-adaptive mesh generator of the Matlab finite elements solver, a first solving of the thermal equation is done and gives the temperature distribution as indicated in *figure 11*. In this figure, it can be noted that the major part of the temperature gradient is in the graphite insulating foam and that the temperature gradient in the graphite crucible is low with a mean value of the temperature of about 1 600 °C, the lower part being slightly hotter than the upper part. The corresponding temperatures T_{A}, T_{B}, T_{C} and T_{D} of the 4 specific points

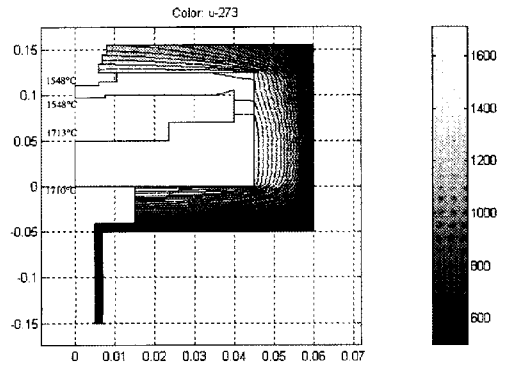

Figure 11. Calculated temperature distribution after first solution.

A, B, C and D of *figure 10* are indicated in *figure 11* and are the following: $T_{\text{A}} = 1\,548$ °C, $T_{\text{B}} = 1\,710$ °C, $T_{\text{C}} = 1\,548$ °C, $T_{\text{D}} = 1\,713$ °C. The temperature at points A and B have also been measured (see section 3, first line of *table III*), showing that the calculated values T_{A} and T_{B} are close to the measured ones with less than 10 % error but with an inverted gradient between A and B. It is clear that these differences depend on the choice of the boundary conditions set of the thermal problem.

In order to improve the accuracy of the results, a second solving is done by adding to the former boundary conditions set a radiative thermal flux generalised Neumann boundary condition on the horizontal faces of the crucible internal chamber (which was insulated for the first solution) corresponding to the couples of faces (CO, PQ) and (DR, ST) which face each other as indicated in *figure 10*. This additional Neumann boundary condition is expressed as $-k\,\vec{n}\,\overrightarrow{\text{grad}}\,T = \varepsilon\,\sigma_{\text{st}}\,(T^4 - T_{\text{ref}}^4)$ in which ε is the emissivity (equal to 1 for the graphite), σ_{st} is the Stefan-Boltzmann constant and T_{ref} is the reference temperature on which the considered face radiates. The reference temperature of the radiative losses of the couple (CO, PQ) is assumed to be the previously calculated average temperature (obtained by the first solution) of the other couple (DR, ST) and reciprocally. This is easily done by entering this additional boundary condition in the Matlab solver on the boundaries corresponding to the couples of faces (CO, PQ) and (DR, ST). This must be considered as a simplified manner of taking into account the 'face to face' radiation losses which exist in the internal chamber of the graphite crucible. The results of this second solution are given in *figure 12* on which the corresponding temperature T_{A}, T_{B}, T_{C} and T_{D} of the 4 specific points A, B, C and D of *figure 10* are indicated. They are the following: $T_{\text{A}} = 1\,706$ °C, $T_{\text{B}} = 1\,573$ °C, $T_{\text{C}} = 1\,713$ °C, $T_{\text{D}} = 1\,554$ °C. It can be noted that the two calculated temperatures T_{A} and T_{B} are quite close to the measured temperatures (see first line of *table III*) with the right gradient this time.

Thus the thermal model is in good agreement with the measurements and the global electromagnetic-

thermal model can be considered as a design and optimisation tool for this kind of inductive process. It must be noted that exact matching between this kind of modelling and the real device is quite difficult to obtain because some data such as, for instance, the thermal boundary conditions, are difficult to evaluate. Therefore this kind of design tool is mainly of interest for studying the relative behaviour variations due to the different parameter variations.

6. CONCLUSION

The work presented in this paper is related to the application of a two-dimensional electromagnetic-thermal coupling model set up with the Matlab finite elements solver for the optimisation of a single SiC crystal inductive elaboration process. The SiC crystal is obtained in a graphite crucible which is heated by induction, after sublimation of the SiC starting powder and condensation on the upper face of the crucible. This optimisation tool is mainly focused on the 'macroscopic' electrical and thermal engineering aspects.

The electromagnetic model using an equation derived from the Maxwell equations and Ohm's law with an imposed inductor voltage gives all the electrical parameters, i.e. the resistance, the inductance and the coupling efficiency of the inductive system. These parameters are in good agreement with the measured values. The real inductor current density distribution is also obtained, showing an uneven distribution with a shift toward the inner faces of the turns. It must be noted that taking into account this real inductor current density, called proximity effects, is important for the accuracy of the induced effects in the different coupling materials such as the graphite crucible and the graphite insulating foam. Finally this model gives the power density distribution in these coupling materials. This power density distribution is then used as the heat source to achieve the coupling with the thermal model.

The thermal model is also solved with the Matlab finite elements solver with an appropriate boundary conditions set including both fixed temperature and thermal flux conditions. This requires the use of the non linear solver, particularly because the insulating foam thermal conductivity is chosen as a function of the temperature. The temperature distribution obtained in the coupling materials such as the graphite crucible is in good agreement with the measured values.

In conclusion, it can be said that the mathematical and graphical efficiency of Matlab associated with its finite elements solver can be considered as a new and original global electrical and thermal optimisation tool which is quite easy to manage for the design or optimisation of middle or high frequency inductive industrial processes. The main inconvenience of this tool is that, compared with other finite elements solvers, it is used as a 'closed box' and so it does not allow the user to control how it works internally from a numerical point of view. But it must be accepted that, thanks to the Windows (and also Unix) working environment, it is quite convenient to use for researchers or engineers and, according to the results presented in this paper, gives good precision for the optimisation of induction processes.

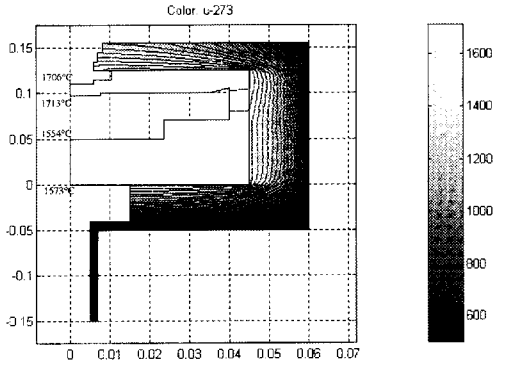

Figure 12. Calculated temperature distribution after second solution.

REFERENCES

[1] Tairov Y.M., Tsvetkov V.F., Investigation of growth processes of ingots of silicon carbide single crystals, J. Crystal Growth 43 (2) (1978) 209.

[2] Hobgood H. McD., Barret D.L., McHugh J.P., Clarke R.C., Sriram S., Burke A.A., Greggi J., Brandt C.D., Hopkins R.H., Choyke W.J., Large diameter 6H–SiC for microwave device applications, J. Crystal Growth 137 (1994) 181.

[3] Takanashi J., Kanaya M., Fujiwara Y., Sublimation growth of SiC single crystalline ingots on faces perpendicular to the (0001) basal plane, J. Crystal Growth 135 (1994) 61.

[4] Garcon I., Rouault A., Anikin M., Jaussaud C., Madar R., Study of SiC single-crystal sublimation growth conditions, Mater. Sci. Eng. B29 (1995) 90.

[5] Zienkiewicz O.C., The Finite Element Method, McGraw Hill, 3rd Edition, 1977.

[6] Irons B., Ahmad S., Techniques of Finite Elements, Ellis Horwood, 1980.

[7] Kriezis E.E., Tsiboukis T.D., Panas S.M., Tegopoulos J.A., Eddy currents: theory and application, Proceedings of the IEEE 80 (10) 1559–1589.

[8] Chaboudez C., Clain S., Glardon R., Rappaz J., Numerical modelling of induction heating of long workpiece, IEEE T. Magn. 30 (6) 5028–5036.

[9] Ernst R., Garnier C., Mesure numérique des caractéristiques d'un circuit oscillant pour le chauffage par induction, Revue Générale de l'Électricité, Sept. 1989.

[10] Pons M., Blanquet E., Dedulle J.-M., Madar R., Bernard C., Thermodynamic heat transfer and mass transport modeling of the sublimation growth of silicon carbide crystals, J. Electrochem. Soc. 143 (11) (1996).